Decolorization of Methylene Blue in an Ar Non-Thermal Plasma Reactor

Khanit Matra* and Sittinum Tawkaew

Electrical Engineering Department, Engineering Srinakharinwirot University, Nakhin Nayok 26120, Thailand

___

Abstract

The decolorization of methylene blue (MB) dye wastewater was performed via atmospheric Ar non-thermal plasma (Ar-NTP). Investigations were carried out into two main aspects of the model; hydrogen peroxide (H_2O_2) production and the decolorization of MB by Ar-NTP. It was found that H_2O_2 could be obtained better at a lower pH and with a higher Ar gas flow rate and plasma power. The decolorization rate constant of MB decreased with the increase in the solution pH, and it was found to follow a pseudo-first-order reaction. The optimum experimental conditions in this paper for the decolorization of a 5 ppm initial MB concentration were: 20.35 W plasma power, 4 LPM Ar gas flow rate, and pH 5, together with the addition of 920 ppm Fe^{2+}. The decorization rate constant was 83.7×10^{-3} min^{-1}, which was 9.73 times greater than that without the addition of Fe^{2+} under the same experimental conditions.

Keywords: Argon plasma, Non-thermal gas discharge, Methylene blue, Decolorization, Water treatment.

___

1. Introduction

Nowadays, dye wastewater is one of most serious problems in Thailand and requires an urgent solution due to its effects on the environment. Dye wastewater treatment can be generally performed utilizing conventional methods, such as filtration, chemical oxidation, Fenton oxidation, and biodegradation [1-5]. It has been reported that the biodegradation method is not suitable for dye wastewater treatment since the dye is toxic to microorganisms. Filtration or the coagulation process does not represent a dye degradation process, but can be used for separating dyes from wastewater to a solid phase. For chemical oxidation and Fenton oxidation, which are considered suitable methods for dye wastewater treatment, an oxidizing agent, such as hydrogen peroxide (H_2O_2), is required for the oxidation process. Moreover, H_2O_2 can produce a hydroxyl radical (•OH), which is another powerful oxidizing agent for dye wastewater treatment [2], [6]. Recently, it was reported that both H_2O_2 and •OH could be produced by a non-thermal plasma technique [7-11].

§Advanced oxidation processes (AOPs) at the interface between plasma and the liquid phase offer some advantages, and among these, atmospheric non-thermal plasma has recently been proposed as a promising technique for wastewater treatment [4], [9], [12-14]. Organic and inorganic matter could be removed from wastewater by oxidation via the reactions with ozone (O_3), H_2O_2, •OH, and/or sulfate radicals (SO_4•−) during the advanced oxidative process [14-16]. These active species can diffuse into the liquid phase, and chemically react with the organic and/or inorganic particles in the wastewater [12-15]. Moreover, owing to beneficial radical production and chemical reactions of AOPs by atmospheric non-thermal plasma, plasma technology has been continuously developed and applied in various fields, such as nanostructure and nanomaterial synthesis, microorganism inactivation, biomedical treatment, agricultural enhancement, and air and water purification [7-8], [11], [17].

This research aimed to investigate the effect of atmospheric Ar non-thermal plasma (Ar-NTP) on the decolorization of methylene blue (MB) dye wastewater. A plasma model was simply designed, with the aim that it could be easily applied in a small dye wastewater treatment system. The electrical characteristics of the Ar-NTP, the discharge current, and the voltage are discussed herein. The influences of the solution pH, Ar gas flow rate, and plasma power on H_2O_2 production, and on the decolorization of MB were studied. The effect of the addition of Fe^{2+} on the decolorization of MB was also investigated.

2. Experimental Methods

2.1 Argon non-thermal plasma reactor setup

A schematic drawing of the utilized Ar non-thermal plasma (Ar-NTP) system for dye wastewater treatment is illustrated in Fig. 1. The treatment system comprised three main parts: the plasma model, gas flow controller, and high-voltage power supply. For the plasma model, 6 pin electrodes with a diameter of 2 mm and length of 5 mm were bonded perpendicularly on a stainless steel rod, with a spacing of 10 mm between two pin electrodes. These pin electrodes were expected to help reduce breakdown voltage for plasma ignitions. The anode electrode was placed in an acrylic cylindrical chamber, which had a radius, thickness, and length of 15, 2, and 100 mm, respectively. There were 6 holes on the surface of the chamber. The diameter of each hole was 1.25 mm. Each hole in the acrylic chamber was located above each pin electrode's tip. The gap between the anode tip and hole was 2.5 mm. A 10×80 mm^2 copper sheet was placed 5 mm above the anode tip and acted as the cathode and ground electrode. Argon (Ar) gas was provided from a gas cylinder with the flow rate controlled by a flow meter, and was fed in to the acrylic chamber via a plastic tube connected at both

sides of the chamber. An in-house resonant AC power source was supplied to the anodes for Ar-NTP generation. The Ar-NTP model was placed in a $10\times30\times20$ cm^3 glass container and immersed under 2 L of MB solution. During the methylene blue treatment, the solution was circulated using a 600 L/h water pump to achieve uniform treatment of the whole volume. In this time, the Ar-NTP was operated for 60 min at various input powers with a frequency around 66 kHz. The root mean square (rms) value and waveform of the discharge current (I_d) and the voltage (V_d) characteristics were inspected using an oscilloscope (Siglent SDS2304). To observe the V_d, a high-voltage probe (Pintek HVP-28HF) was connected across the Ar-NTP reactor. A one $k\Omega$ monitoring resistor was placed between the cathode and ground for the I_d measurement.
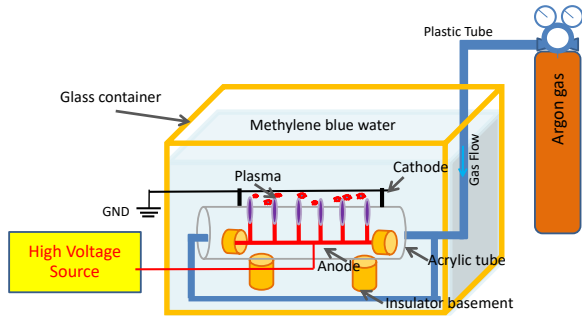

Fig. 1. (Color online) Plasma generation under MB wastewater.

2.2. Measurement procedures for hydrogen peroxide production and the decolorization of methylene blue

The concentration of H_2O_2 production was measured via the developing color during the reaction of H_2O_2 and the metavanadate ion (VO_3^-) as shown in Eq. 1. H_2O_2 reacts with the metavanadate anion (VO_3^-) in acid solution to form the peroxovanadium cation (VO_2^{3+}). This measurement technique was modified from Nogueira et al. and Mahadevaiah et al [18-19]. Typically, 10 mL of the sample was taken, and the color developed upon the addition of 5 mL of 0.015 M ammonium metavanadate (NH_4VO_3) and 5 mL of 3 M H_2SO_4. The solution was then made up with distilled water to a final volume of 25 mL. The concentration of H_2O_2 was measured at $\lambda_{max} = 450$ nm with a T80+ UV-VIS spectrophotometer (PG Instruments Ltd.). A blank solution was prepared as a control following the same procedure as that for the developed color process, but distilled water was used instead of the sample

$$VO_3^- + 4H^+ + H_2O_2 \rightarrow VO_2^{3+} + 3H_2O \qquad (1)$$
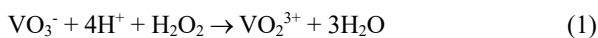
For assessing the efficiency of MB treatment, the decolorization of the MB dye solution was measured with a T80+ UV-VIS spectrophotometer (PG Instruments Ltd.). The concentration of the dye was determined from the measured UV-VIS spectrum, using the maximum MB absorption at $\lambda_{max} = 660$ nm.

3. Results and discussion

3.1 Plasma and electrical characteristics

Since the high-voltage source used was a resonant AC power source, the output voltage was influenced by the resistance, capacitance, and inductance of the plasma model, as well as the Ar gas flow rate. Therefore, the input power of the power source was used as a control parameter for convenience. In this paper, Ar-NTP was operated at the input power of 60, 80, and 100 W with a frequency around 66 kHz. The Ar gas flow

rate was varied form 2 to 4 liter per minute (LPM). When the power source was applied to the plasma reactor, Ar-NTP under the methylene blue water was generated between the anode tip and methylene blue water. Fig. 2 shows an image of Ar-NTP generation under MB water. The plasma jet color was bright purple-blue. Six streamer-like plasma jets originate from the six anode pins, and inject through the holes of the Ar-NTP reactor into the MB water. The characteristics of plasma jets were a self-sustained AC corona discharge [20-23]. From the experimental results, it was found that the longest and brightest plasma jets' lengths were found with the input power of 100 W and a 4 LPM Ar gas flow rate, which were 1.25 cm, approximately. The diameter of the plasma jets was a little larger than the diameter of the anode pin. It could be observed that at the higher gas flow rate and input power, plasma jets could expand and inject into the solution better. While the plasma jets elongated and reached just around the exit holes of the Ar-NTP reactor for other cases. The temperatures of treated solution after 60 min treatment had just slightly increased from the temperatures of solution before treatment.
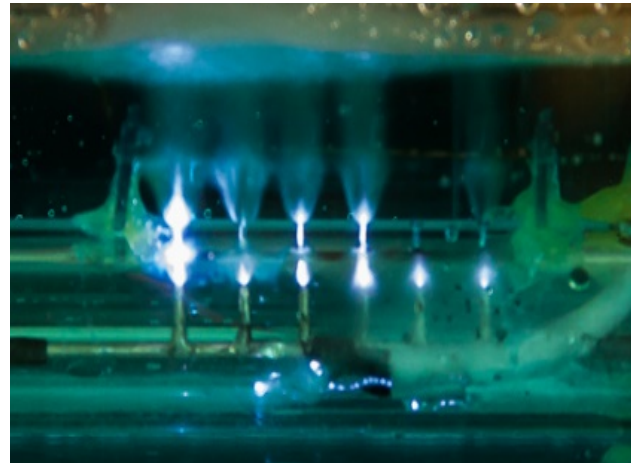

Fig. 2. (Color online) Ar-NTP generation under MB wastewater at an input power of 100 W and an Ar gas flow rate of 4 LPM.

An example of the discharge voltage and current waveforms during Ar-NTP generation under MB wastewater is presented in Fig. 3. The discharge waveforms under the other experimental conditions were also observed with similar characteristics, but the magnitudes of the parameters were different depending on the gas flow rate and power source input power. Owing to there being multi-anode pins, each anode pin generated its own discharge. Therefore, numerous micro discharge current pulses on each cycle could be noticed [12-13], [24-27]. The electrical discharge parameters of Ar-NTP generation under the various conditions are shown in Tab. 1. It was noticed that at the same gas flow rate, the output power, I_d, and V_d were slightly increased when the input power was increased, while at the same input power, the output power decreased when the gas flow rate was increased. Under the condition, in which Ar-NTP could be generated the most (as noted by the observed size and brightness of the plasma), the discharge current, voltage, and output power or plasma power were 48.56 mA$_{rms}$, 419.1 V$_{rms}$, and 20.35 W, respectively.

3.2 Influence of the plasma power and gas flow rate on the hydrogen peroxide production rates

The influence of the Ar-NTP generating power and Ar gas flow rate on hydrogen peroxide (H_2O_2) production were investigated. Fig. 4a presents the effect of the Ar gas flow rate

on H_2O_2 production with a fixed input power of 100 W, and at pH 7 of the MB water. The experimental results showed that an increase in the Ar gas flow rate could increase the concentration of H_2O_2. The highest H_2O_2 concentration was found with the largest Ar gas flow rate, namely 4 LPM. The H_2O_2 concentration in solution after 60 min treatment was 9.53×10^{-3}, 12.53×10^{-3}, and 14.81×10^{-3} ppm at Ar gas flow rates of 2, 3 and 4 LPM, respectively. The concentration of H_2O_2 with the Ar gas flow rates of 3 and 4 LPM was improved by about 1.31 and 1.55 times that at 2 LPM, respectively.

Table 1. Discharge voltage and current for Ar-NTP generation under various conditions

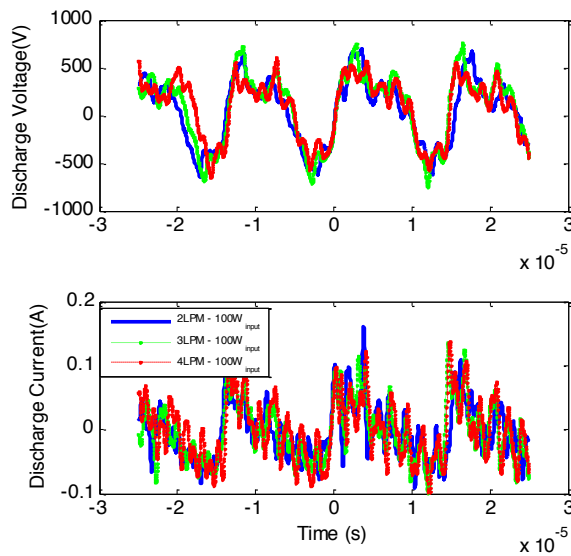| Argon gas flow rate (LPM)	Input power of power source (W)	Output power (plasma power, W)	Discharge voltage (V$_{rms}$)	Discharge current (mA$_{rms}$)
2	60	15.39	364.1	42.27
	80	15.87	369.1	43.01
	100	16.39	373.1	43.94
3	60	15.32	350.2	43.76
	80	16.65	379.9	43.83
	100	18.23	395.2	46.12
4	60	14.60	333.0	43.84
	80	18.86	393.5	47.93
	100	20.35	419.1	48.56

Fig. 3. (Color online) Real-time discharge voltage and current waveforms during Ar-NTP generation under MB wastewater at a 100 W input power and various gas flow rates.
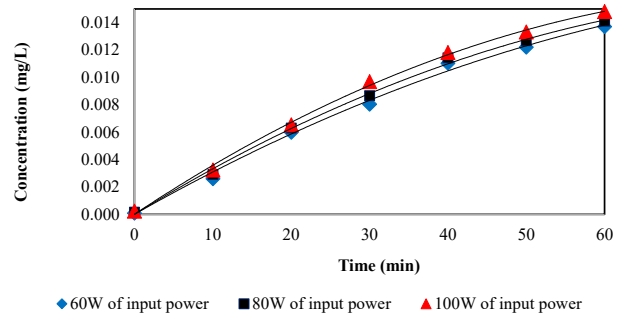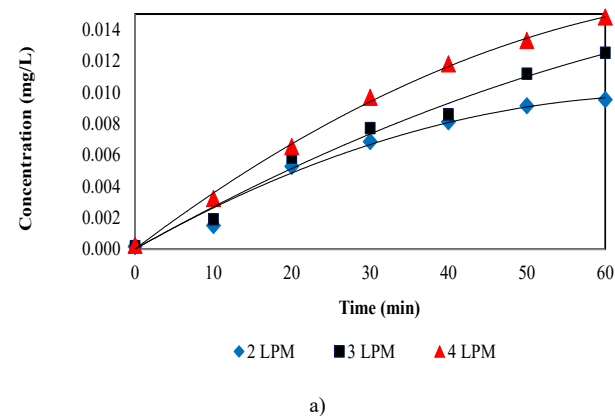

a)

b)

Fig. 4. (Color online) a) Influence of the Ar flow rate at 100 W input power, and b) influence of plasma power at an Ar flow rate of 4 LPM on H_2O_2 production.

The evolution of H_2O_2 production as a function of plasma power at an Ar gas flow rate of 4 LPM is shown in Fig. 4b. It was expected that the concentration of H_2O_2 would be enhanced by increasing the plasma power as a result of the chemical equilibrium between the formation and destruction of H_2O_2 [28-30]. From the experimental results, it was indeed seen that an increase in the input power from 60 to 80 and 100 W could enhance the concentration of H_2O_2 in solution, with the H_2O_2 concentrations after 60 min treatment in each case 13.71×10^{-3}, 14.10×10^{-3}, and 14.81×10^{-3} ppm, respectively. However, it was noticed that the input power did not significantly affect the H_2O_2 production. This could possibly be due to the poor efficiency of the in-house power source, as could be noticed in Tab. 1. The output power of each input power was just about 25% of the input power, which hence needs to be improved. Since the increase in input power resulted in a slight difference in the output power, the H_2O_2 production was not significantly improved. However, the highest H_2O_2 concentration was found with the largest input power; therefore, this input power (100 W) was used for the rest of the experiments.

The principal oxidative species formed in the gas phase by the discharge are hydroxyl radicals ($\bullet$OH) and hydrogen peroxide (H_2O_2) [31-34]. The dominant reactions that take place in the plasma-liquid interface are listed as follows:
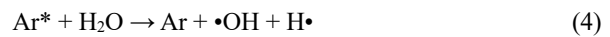
Excitation of Ar with a free electron

$$e^- + Ar \rightarrow Ar^* + e^- \tag{2}$$

Interact of water with an electron

$$H_2O + e^- \rightarrow H\bullet + \bullet OH + e^- \tag{3}$$

Generation of radicals

$$Ar^* + H_2O \rightarrow Ar + \bullet OH + H\bullet \tag{4}$$

H_2O_2, H_2, and O_2 production

$$H\bullet + H\bullet \rightarrow H_2 \tag{5}$$

$$HO\bullet + HO\bullet \rightarrow H_2O_2 \tag{6}$$

$$HO\bullet + H_2O_2 \rightarrow HO_2\bullet + H_2O \tag{7}$$

$$2HO_2\bullet \rightarrow H_2O_2 + O_2 \tag{8}$$

$$H\bullet + O_2 \rightarrow HO_2\bullet \tag{9}$$

$$H_2 + HO\bullet \rightarrow H_2O + H\bullet \qquad (10)$$

$$HO\bullet + H\bullet \rightarrow H_2O \qquad (11)$$

Ar* is generated during the plasma process (reaction in Eq. 2), and then reacts with interfacial water to generate hydrogen radical (H•), and hydroxyl radical (•OH) (reaction in Eq. 4). Houria Ghodbane et al. suggested that the reaction in Eq. 2 is faster than the reaction in Eq. 3 for the generation of •OH radicals in argon-water vapor mixtures [32]. The increase in the Ar gas flow rate could increase the concentration of Ar gas, which contribute to Ar* production enhancement. The main reactions for H_2O_2 production are shown in Eq. 6, and Eq. 8. Joshi et al. suggested that that the reaction rate for the production of H_2O_2 obeys the zero-order rate law since the concentrations of Ar and water in reaction in Eq. 4 are constant during the experiment [31]. In addition, Liu et al. reported that the production rate of H_2O_2 depended on the applied current and voltage of the plasma source [2].

3.3 Influence of solution pH on H_2O_2 production.

The influence of the pH of the solution on H_2O_2 production was also investigated at pH 5, 7, and 9. In this part, the Ar-NTP generating plasma power and the Ar gas flow rate were fixed at 20.35 W and 4 LPM, respectively, due to the highest H_2O_2 production rate being obtained under these conditions as presented in the last section. The results of this experiment are shown in Fig. 5. The concentrations of H_2O_2 after 60 min treatment were 15.60×10^{-3}, 14.50×10^{-3}, and 13.47×10^{-3} ppm at pH 5, 7, and 9, respectively. It was noticed that a decrease in the solution pH seemed to enhance the production rate of H_2O_2. This is due to the fact that the low pH solution contains a high amount of H^+ species in solution, which causes an increase in the electrical conductivity of the solution, and an enhancement of the reaction between the generated free electrons during plasma generation with the MB solution (reaction in Eq. 3). This factor could improve the H_2O_2 production rate [28].
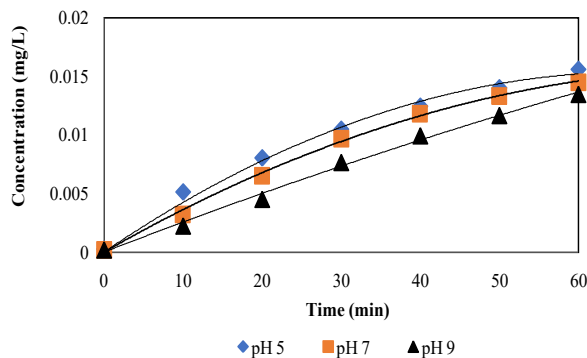
Fig. 5. (Color online) Influence of MB solution pH on H_2O_2 concentration.

3.4 Degradation of MB concentration

To observe the degradation efficiency of the MB concentration after Ar-NTP treatment in the previous section, the MB solutions were analyzed by recording their UV–visible spectra. Fig. 6 presents the UV–visible spectra of the untreated and treated MB solution with the initial MB concentration of 5 mg/L. The experiment conditions for the treated MB solution were 20.35 W plasma power and 4 LPM Ar gas flow rate. The absorbance of the treated MB solution decreased after Ar-NTP treatment for 60 min. Here, the spectra of MB showed strong absorption peaks in the visible spectral region with λ_{max} at 660 nm and in the other two

spectra in the UV region with λ_{max} at 291 and 246 nm. The peaks at 660 nm correspond to n-π* transitions (n is the free doublet on the nitrogen atom of a C=N bond and the free doublet of a S atom on a S=C bond). Other peaks at 291 and 246 nm correspond to π-π* transitions of the benzene ring. After Ar-NTP treatment for 60 min, the peak intensity at 660, 291, and 246 nm decreased. This confirmed that the Ar-NTP treatment could enhance the degradation of MB. The MB degradation mechanism could be explained as following two pathways [28], [30], [32]. The first pathway is where high energetic electrons react with MB molecules, resulting in breaking down the chemical bonds in MB; for example, the –$N\text{-}(CH_3)_2$ group is broken down to form an –$N\text{-}H(CH_3)$ group. The second pathway is where •OH reacts with MB molecules, resulting in breaking down the structural rings of MB molecules at the C–S and C–N bonds, causing the MB molecule to become two-parts of small molecules [33].
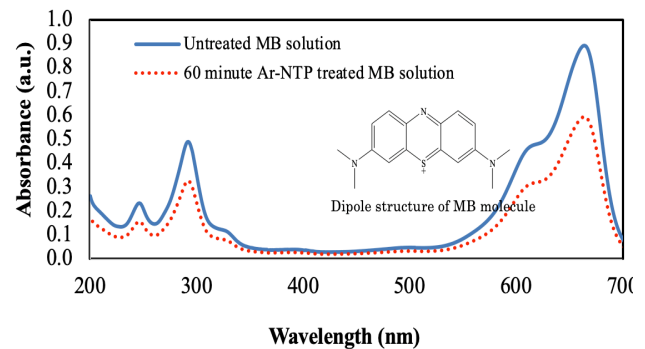
Fig. 6. (Color online) UV–visible spectra of MB aqueous solution before and after 60 min Ar-NTP treatment.

Fig. 7a shows the results of the effect of pH on the decrease in MB concentration. At a treatment time of 60 min, the remaining concentration of MB at pH 5 was the lowest. The degradation of MB at pH 5, 7, and 9 was 17%, 13%, and 10%, respectively. These low degradations of MB may be due to the low plasma power. To determine the degradation rate constant of MB, the experimental results from Fig. 7a were plotted as a function of $\ln(C_{MB})$ and the treatment time, where C_{MB} is the methylene blue concentration. The slopes of each plot represent the degradation rate constants of MB, which are presented in Fig. 7b. It was found that at a low pH, the degradation rate constant was higher than that at a high pH. The degradation rate constants at pH 5, pH 7, and pH 9 were 8.6×10^{-3}, 5.90×10^{-3}, and 4.20×10^{-3} min^{-1}, respectively. The degradation rate constant at pH 5 was about two times the degradation rate constant at pH 9. At a lower pH, the generation rate of H_2O_2, which plays an important role in MB degradation, was higher than that at the higher pH [34]. The MB degradation followed a pseudo-first-order reaction caused by the reaction between the high energetic electron, the hydroxyl radical (•OH), and H_2O_2 with the MB molecule [28].
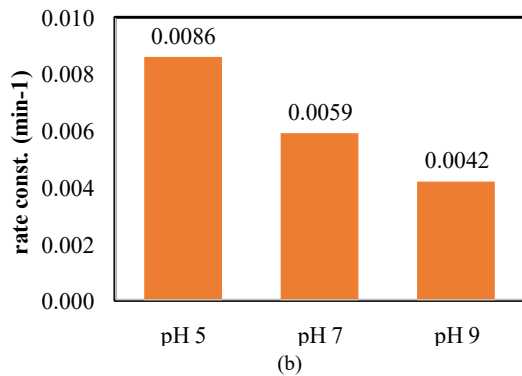
(a)
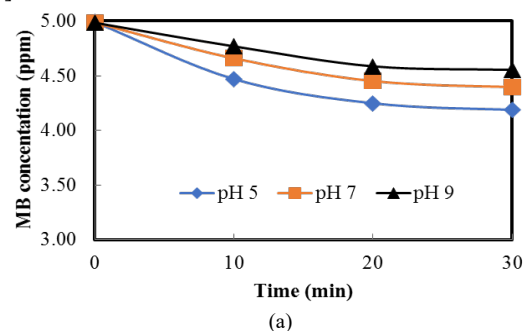
Fig. 7. (Color online) a) Concentration of MB, and b) the reaction rate of degradation of MB at various pH values after Ar-NTP treatment.

3.5 MB degradation enhancement by the addition of Fe^{2+}

The effect of the addition of Fe^{2+} on MB degradation enhancement was studied. Fe^{2+} was added to the pH 5 MB solution with an initial MB concentration of 5 ppm. Ar-NTP treatment was performed at a plasma power of 20.35 W and Ar gas flow rate of 4 LPM. Fig. 8a presents the degradation rate constant of MB with various Fe^{2+} concentrations (0–3680 mg/L). The degradation rate constant linearly increased with increasing the concentration of the added Fe^{2+}. It was noticed that the degradation rate constant seemed to become saturated at 83.7×10^{-3} min^{-1} when the addition concentration of Fe^{2+} was more than 920 mg/L. Therefore, the proper addition amount of Fe^{2+} for optimized MB degradation in this experiment was determined to be 920 mg/L. Fig. 8b illustrates the MB solutions with a 5 ppm initial MB concentration after Ar-NTP treatment at the different treatment times of 0, 10, 20, 30, 40, 50, and 60 min.
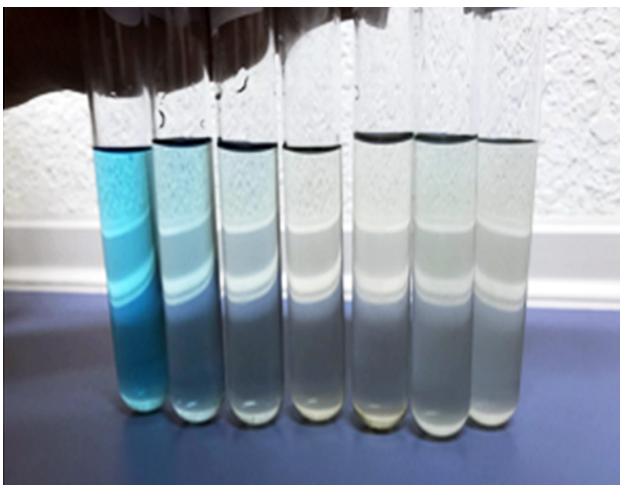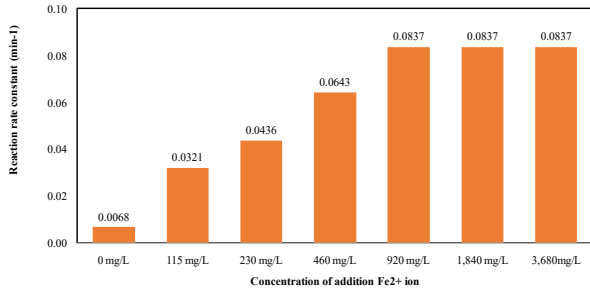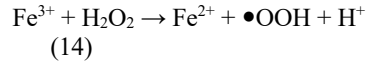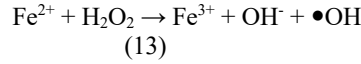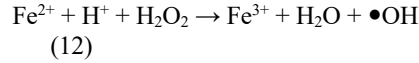

Fig. 8. (Color online) a) Degradation rate constant of MB with the addition of Fe^{2+} at various initial MB concentrations, and b) MB solutions with 5 ppm of initial MB concentration after Ar-NTP treatment at different treatment times: 0, 10, 20, 30, 40, 50, and 60 min (from left to right). The Ar-NTP treatments were performed at a plasma power of 20.35 W, 4 LPM Ar gas flow rate, and pH 5 for the MB solution.

In the Fenton process, H_2O_2 can be easily decomposed to $\bullet OH$ in the presence of Fe^{2+} ions. The Fe^{2+} ion reacts with H_2O_2 to form $\bullet OH$ and Fe^{3+}, as shown in the reaction in Eq. 12–14 [35]. The generated Fe^{3+} then reacts with H_2O_2 to form $\bullet OH$ and perhydroxide radical ($\bullet OOH$) [36-37]. Here, $\bullet OH$ is a stronger oxidizing agent for MB degradation than H_2O_2. Therefore, the addition of Fe^{2+} into the MB solution would improve the degradation rate of MB.

$$Fe^{2+} + H^+ + H_2O_2 \rightarrow Fe^{3+} + H_2O + \bullet OH \quad (12)$$

$$Fe^{2+} + H_2O_2 \rightarrow Fe^{3+} + OH^- + \bullet OH \quad (13)$$

$$Fe^{3+} + H_2O_2 \rightarrow Fe^{2+} + \bullet OOH + H^+ \quad (14)$$

To determine the effect of the initial concentration of MB on the degradation rate constant, the initial concentration of MB was varied at 5, 10, 15, and 20 ppm. Ar-NTP treatment was performed for 60 min at 20.35 W plasma power, 4 LPM Ar gas flow rate, pH 5, and with the addition of 920 mg/L of Fe^{2+}. From the experimental results, the degradation rate constant of MB was seen to decrease with the increase in the initial MB concentration, as depicted in Fig. 9. The degradation rate constants for the initial concentrations of MB at 5, 10, 15, and 20 ppm were 0.0551, 0.279, 0.0182, and 0.0119 min^{-1}, respectively. This could imply that a high initial concentration of MB needs more treatment time for the plasma treatment [38].
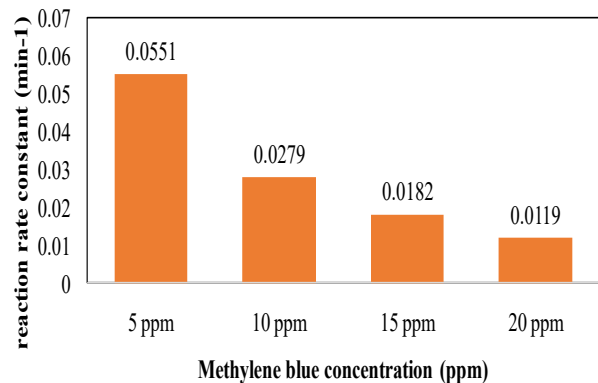

Fig. 9. (Color online) Degradation rate constant of MB with the addition of 920 mg/L Fe^{2+} ions at various initial MB concentrations.

4. Conclusions

An investigation was carried out into the influence of Ar non-thermal plasma (Ar-NTP) on the decolorization of methylene blue (MB) and the results presented herein. It was confirmed that the flow rate of Ar gas and the plasma power significantly affected the production of hydrogen peroxide (H_2O_2). The results showed that increasing the Ar gas flow rate and the plasma power resulted in an increase in H_2O_2 production. Also, the production of H_2O_2 was greater at lower pH. The decolorization rate constant of MB followed a pseudo-first-order reaction, and decreased with the increase in solution pH. The addition of Fe^{2+} ions could enhance the decolorization rate of MB. The optimum experimental conditions for the decolorization of a 5 ppm initial MB concentration without the addition of Fe^{2+} were 20.35 W plasma power, 4 LPM Ar

gas flow rate, and pH 5, which resulted in a decolorization rate of 8.6×10^{-3} min^{-1}. Whereas, the decolorization rate increased 9.73 times when 920 ppm of Fe^{2+} was added to the MB solution.

References

1) K. Takahashi, K. Takaki, and N. Satta, J. Adv. Oxid. Technol. **15**, (2012).
2) J. Liu, B. He, Q. Chen, J. Li, Q. Xiong, G. Yue, X. Zhang, S. Yang, H. Liu, and Q. H. Liu, Scientific Reports **6**, (2016).
3) J. Gao, Pak. J. Biol. Sci. **9**, 323 (2006).
4) T. C. Shih, M. Wangpaichitr, and M. Suffet, Water Research **37**, 375 (2003).
5) B. Jiang, J. Zheng, S. Qiu, M. Wu, Q. Zhang, Z. Yan, and Q. Xue, Chem. Eng. J. **236**, 348 (2014).
6) J.P. Bruggeman and D.C. Schram, Plasma Sources Sci. Technol. **19**, 045025 (2010).
7) D.B. Graves, J. Phys. D 45, 263001 (2012).
8) N. Khamsen, O. Damrongvudhi, T. Nithiphat, S. Dechanupaprittha, W. Kanokbannakorn, K. Hongesombut, and S.Srisonphan. ACS Appl. Mater. Interfaces **8**, 19268 (2016).
9) B. Jiang, J. Zheng, S. Qiu, M. Wu, Q. Zhang, Z. Yan, and Q. Xue, Chem. Eng. J. **236**, 348 (2014).
10) Y. Gorbanev, D. Oconnell, and V. Chechik, Chem. Eur. J. **22**, 3496 (2016).
11) T.G. Klampfl, G. Isbary, T. Shimizu, Y.-F. Li, J.L. Zimmermann, W. Stolz, J. Schlegel, G.E. Morfill, and H.-U. Schmidt, Appl. Environ. Microbiol. **78**, 5077 (2012).
12) S. Theepharaksapan and K. Matra, The 2018 International Electrical Engineering Congress (iEECON2018), IEEE, (2018). [in Press]
13) C. Dechthummarong and K. Matra, The 2018 International Electrical Engineering Congress (iEECON2018), IEEE, (2018). [in Press]
14) H.H. Cheng, S.S. Chen, Y.C. Wu, and D.L. Ho. J. Environ. Eng. Manage. **17**, 427 (2007).
15) S. Katsuki, K. Tanaka, T. Fudamoto, T. Namihira, H. Akiyama, and H. Bluhm, Jpn. J. Appl. Phys. **45**, 239 (2006).
16) X. Liao, D. Liu, Q. Xiang, J. Ahn, S. Chen, X. Ye, and T. Ding, Food Control **75**, 83 (2017).
17) K. Panngom, S.H. Lee, D.H. Park, G.B. Sim, Y.H. Kim, H.S. Uhm, G. Park, and E.H. Choi, PLOS ONE **9**, (2014).
18) R. Nogueira, M. Oliveira, and W. Paterlini, Talanta **66**, 86 (2005).
19) M. S. Mahadevaiah, A. Galil, M. S. Y. Kumar, M. A. Sathish, and G. Nagendrappa, J. Anal. Chem. **63**, 239 (2008).
20) K. Matra, Jpn. J. Appl. Phys. **57**, (2017).
21) R. Morrow, J. Phys. D **30**, 3099 (1997).
22) R. Ono, Y. Nakagawa, and T. Oda, J. Phys. D **44**, 485201 (2011).
23) H. Taghvaei and M.R. Rahimpour, RSC Adv. **6**, 98369 (2016).
24) C. Lazzaroni and P. Chabert, Plasma Sources Sci. Technol. **20**, 055004 (2011).
25) K. Matra, H. Furuta, and A. Hatta, J. Phys.: Conf. Ser. **441**, 012021 (2013).
26) J. Choi, K. Matsuo, H. Yoshida, T. Namihira, S. Katsuki, and H. Akiyama, Jpn. J. Appl. Phys. **47**, 6459 (2008).
27) K. Matra, Jpn. J. Appl. Phys. **55**, 07LB02 (2016).
28) L. O. D. B. Benetoli, B. M. Cadorin, V. Z. Baldissarelli, R. Geremias, I. G. D. Souza, and N. A. Debacher, J. Hazard. Mater. **237-238**, 55 (2012).
29) C. A. Vasko, D. X. Liu, E. M. V. Veldhuizen, F. Iza, and P. J. Bruggeman, Plasma Chem Plasma Process **34**, 1081 (2014).
30) M. Magureanu, C. Bradu, D. Piroi, N. B. Mandache, and V. Parvulescu, Plasma Chem Plasma Process **33**, 51 (2013).
31) A.A. Joshi, B.R. Locke, P. Arce, and W.C. Finney, J. Hazard. Mater. **41**, 3 (1995).
32) H. Ghodbane, O. Hamdaoui, J. Vandamme, J. V. Durme, P. Vanraes, C. Leys, and A. Y. Nikiforov, Open Chem. **13**, 325 (2015).
33) G. R. Dey and T. N. Das, Plasma Chem. Plasma Process. **36**, 523 (2015).
34) Y. Wen, J. Yi, S. Zhao, S. Jiang, Y. Chi, and K. Liu, J. Environ. Sci. **44**, 99 (2016).
35) S. Yang, H. He, D. Wu, D. Chen, X. Liang, Z. Qin, M. Fan, J. Zhu, and P. Yuan, Appl. Catal., B **89**, 527 (2009).
36) L. Tengrui, A. Al-Harbawi, Z. Jun, and L. M. Bo, J. Appl. Sci. **7**, 724 (2007).
37) A. Bach, H. Shemer, and R. Semiat, Desalination **264**, 188 (2010).
38) R. F. Quadrado and A. R. Fajardo, Carbohydr Polym. **177**, 443 (2017).